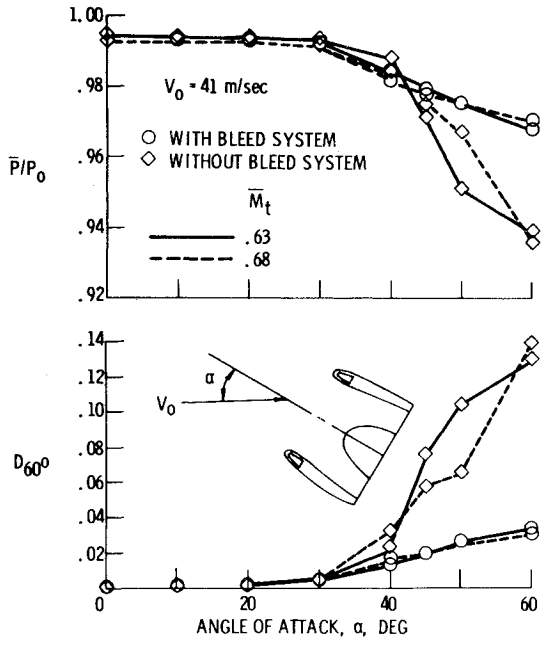

Fig. 3 Improvement in total pressure recovery and reduction of distortion obtained with bleed system.

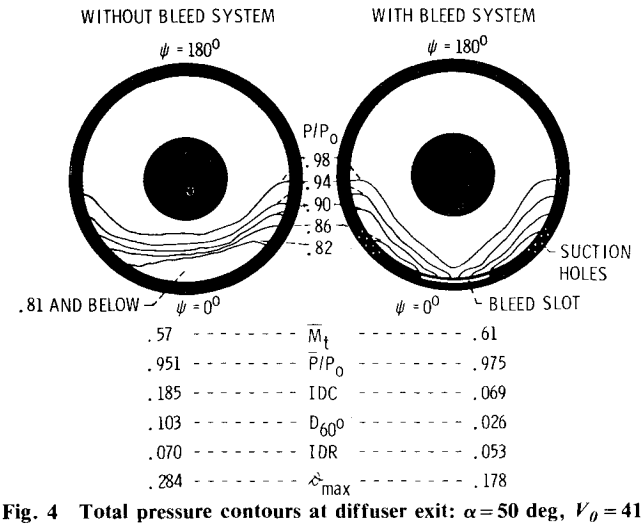

Fig. 4 Total pressure contours at diffuser exit: $\alpha = 50$ deg, $V_0 = 41$ m/sec.

bleed slot within the diffuser is downstream (to the right) of the throat plane. Note that circumferential positions then available on the lip for the low-pressure suction source were limited in the direction of higher values of ψ by a diminishing differential pressure, and in the direction of lower values of ψ by the possibility of developing a recirculating flow between the intake slot and the exit holes. The position selected for the two rows of suction holes represents a compromise between these two extremes. The axial location and spacing of the holes were chosen to reduce the differential pressure between the rows so that locally recirculating flow would be avoided.

Results

The improvement in pressure recovery and reduction of diffuser exit distortion obtained with the bleed system are shown in Fig. 3 as a function of angle of attack. Data for two values of average throat Mach number show a clear advantage with the bleed system for angles above approximately 40 deg. At lower angles performance was unaffected. This apparent lack of a performance penalty at low angles is attributed to reduced bleed flow owing to the much diminished differential pressure between the lip and throat region.[6] The bleed system thus tends to be somewhat self-adaptive by increasing or decreasing the amount of boundary-layer control depending upon the magnitude of the differential pressures, or adverse pressure gradients, that exist within the inlet.

The diffuser exit total pressure contours of Fig. 4 present a graphic picture of the improved flow obtained with the bleed system. The left-hand contour, obtained without bleed, shows a large region of total pressure loss centered about the most windward position ($\psi = 0$). This resulted from diffuser flow separation. The right-hand contour with bleed shows much higher pressure in this region, indicating fully attached, or nearly fully attached flow. The regions of relatively modest total pressure loss to either side of the windward position reflect the diffuser boundary layer ejected back into the inlet through the holes on the lip.

In addition to throat Mach number and pressure recovery, Fig. 4 also lists several distortion indices to permit a quantitative comparison of the two patterns. Circumferential distortion, as defined by IDC and D_{60^0}, was reduced approximately three- to four-fold with the bleed system. Radial distortion, IDR, was reduced 25% while the maximum overall distortion, D_{max}, was reduced approximately 40%.

The lack of rotating machinery with the present model precluded making any measurement to assess what impact, if any, the bleed system might have on fan or compressor noise generation.

Concluding Remarks

The encouraging results presented here suggest that this self-bleeding method for boundary-layer control might be successfully applied to other inlets operating at extreme aerodynamic conditions. Additionally, the flow stabilization possible with this concept could be used to design new shorter, lighter, induction systems that would otherwise suffer flow separation at normal conditions. Although analysis of inlet potential flow will serve as a guide in selecting locations for the bleed and suction ports, detail design of the bleed system will likely require trial and error testing to obtain optimum results.

References

[1] Moore, M.T., "Distortion Data Analysis," General Electric Co., Cincinnati, Ohio, AFAPL-TR-72-11 (AD-756481), Feb. 1973.

[2] Fukuda, M.K., Reshotko, E., and Hingst, W.R., "Control of Shock-Wave Boundary-Layer Interaction by Bleed in Supersonic, Mixed Compression Inlets," AIAA Paper 75-1182, Anaheim, Calif., 1975.

[3] Jakubowski, A.K. and Luidens, R.W., "Internal Cowl Separation at High Incidence Angles," AIAA Paper 75-64, Pasadena, Calif., 1975.

[4] Albers, J.A., "Predicted Upwash Angles at Engine Inlets for STOL Aircraft," NASA TM X-2593, 1972.

[5] Albers, J.A. and Stockman, N.O., "Calculation Procedures for Potential and Viscous Flow Solutions for Engine Inlets," ASME Paper 74-GT-3, 1974.

[6] Albers, J.A. and Miller, B.A., "Effect of Subsonic Inlet Lip Geometry on Predicted Surface and Flow Mach Number Distributions," NASA TN D-7446, 1973.

Applications of an Improved Nonlinear Lifting-Line Theory

C. Edward Lan* and Manuel H. Fasce†
University of Kansas, Lawrence, Kansas

Introduction

PRANDTL'S lifting-line theory has been well developed in the past to allow the use of nonlinear section data in the

Received Oct. 7, 1976.
Index category: Aircraft Aerodynamics (including Component Aerodynamics).

*Associate Professor, Dept. of Aerospace Engineering. Member AIAA.
†Graduate Student; now with Cordiplan Aeronautics, Venezuela. Member AIAA.

calculation of aerodynamic characteristics of high-aspect-ratio, unswept wings.[1,2] Extensive applications of Prandtl's theory have been recently reported.[3,4] As is well known, Prandtl's theory represents the first approximation in the asymptotic expansion for high aspect ratios in the wing theory. As such, its application is limited to high-aspect-ratio wings without sweep. On the other hand, Weissinger's lifting-ling theory[5] and the general lifting-surface theory are capable of treating any aspect-ratio wings. However, both are essentially linear theories and do not permit the use of nonlinear section data without empirical assumptions.

To improve Prandtl's nonlinear lifting-line theory for moderate aspect-ratio wings, an improved theory was presented in Ref. 6. It was shown there how Prandtl's theory could be improved for unswept wings by including higher order terms in the asymptotic expansion of Weissinger's downwash expression for large aspect ratio. The main purpose was to derive a more accurate theory that still allows the use of nonlinear section data. In this Note, the theory of Ref. 6 will be extended to swept wings and some numerical results presented. The detail can be found in Ref. 7.

Method of Analysis

According to the nonlinear lifting-line theory, the sectional circulation, $\Gamma(y)$, is related to the sectional lift coefficient through the following expressions.[6]

$$\beta\Gamma(y)=c(y)\ c_l(y,\ \alpha_e)/2 \tag{1}$$

$$\alpha_e(y)=\alpha(y)+w(x,y,0) \tag{2}$$

where α_e and α are the effective and geometric angles of attack, respectively, $w(x,y,0)$ is the nondimensional downwash referred to the freestream and is positive for upwash, $c(y)$ is the local chord length, and $\beta=(1-M^2)^{1/2}$. To find $w(x,y,0)$, the following Weissinger's velocity potential is used.[6]

$$\phi_w(x,y,z)=\frac{1}{8\pi}\int_{-1}^{1}\frac{2\Gamma(\eta)z}{(y-\eta)^2+z^2}\times\left\{1+\frac{x-\xi}{[(x-\xi)^2+\beta^2(y-\eta)^2+\beta^2z^2]^{1/2}}\right\}d\eta \tag{3}$$

where all physical quantities have been referred to the semispan and freestream velocity. According to Weissinger's method, the lifting line is to be placed along the quarter-chord line of the wing and the boundary condition is satisfied along the three quarter-chord line. It follows that

$$\xi=-c_r/4+|\eta|\tan\Lambda=-f(\eta)-c(\eta)/4+|\eta|\tan\Lambda \tag{4}$$

$$x=-c_r/4+c(y)/2+|y|\tan\Lambda \tag{5}$$

where the coordinate origin is assumed at the midroot chord, and

$$f(\eta)=c_r/4-c(\eta)/4=c_r(1-\lambda)\,|\eta|/4 \tag{6}$$

and c_r is the root chord, λ the taper ratio, and Λ the quarter-chord sweep angle. Using Eq. (4) in Eq. (3) and expanding the result asymptotically for small $c(\eta)/4$, the following expression up to the first order in $c(\eta)/4$ can be obtained.

$$\phi_w(x,y,z)\approx\frac{1}{4\pi}\int_{-1}^{1}\frac{\Gamma(\eta)z}{(y-\eta)^2+z^2}\times\left\{1+\frac{x-|\eta|\tan\Lambda+f(\eta)}{[(x-|\eta|\tan\Lambda+f(\eta))^2+\beta^2(y-\eta)^2+\beta^2z^2]^{1/2}}+\frac{c(\eta)}{4}\frac{\beta^2(y-\eta)^2+\beta^2z^2}{[(x-|\eta|\tan\Lambda+f(\eta))^2+\beta^2(y-\eta)^2+\beta^2z^2]^{3/2}}\right\}d\eta \tag{7}$$

To find the downwash, Eq. (7) is differentiated with respect to z and then z is set to zero to obtain the downwash on the wing plane.

$$w(x,y,0)\approx\frac{1}{4\pi}\int_{-1}^{1}\frac{\Gamma(\eta)}{(y-\eta)^2}\times\left\{1+\frac{x-|\eta|g}{[(x-|\eta|g)^2+\beta^2(y-\eta)^2]^{1/2}}+\frac{c(\eta)}{4}\frac{\beta^2(y-\eta)^2}{[(x-|\eta|g)^2+\beta^2(y-\eta)^2]^{3/2}}\right\}d\eta \tag{8}$$

where

$$g=\tan\Lambda-c_r(1-\lambda)/4 \tag{9}$$

Equation (8) represents the improved downwash expression of the present theory. It differs from Prandtl's theory in the appearance of the second and the third terms in the integrand. For numerical convenience, Eq. (8) is integrated by parts to give[7]

$$w(x,y,0)\approx-\frac{1}{4\pi}\int_{0}^{1}\frac{\Gamma'(\eta)}{y-\eta}P(\eta)d\eta-\frac{1}{4\pi}\int_{-1}^{0}\frac{\Gamma'(\eta)}{y-\eta}Q(\eta)d\eta \tag{10}$$

where

$$\begin{aligned}P(\eta)=1&+\frac{[(x-\eta g)^2+\beta^2(y-\eta)^2]^{1/2}}{x-yg}\\&-2g\frac{[x^2+\beta^2y^2]^{1/2}}{x^2-y^2g^2}(y-\eta)\\&+\frac{c(0)}{2}gx\frac{x^2+2\beta^2y^2+y^2g^2}{(x^2-y^2g^2)^2[x^2+\beta^2y^2]^{1/2}}(y-\eta)\\&-\frac{c'(\eta)}{2}\frac{x^2+y^2g^2}{(x^2-y^2g^2)^2}(x^2+\beta^2y^2)^{1/2}(y-\eta)\\&-\frac{c(\eta)}{4}\frac{\beta^2(y-\eta)-\eta g^2+xg}{(x-yg)^2[(x-\eta g)^2+\beta^2(y-\eta)^2]^{1/2}}(y-\eta)\\&-\frac{c'(\eta)}{4}\frac{[(x-\eta g)^2+\beta^2(y-\eta^2]^{1/2}}{(x-yg)^2}(y-\eta)\end{aligned} \tag{11}$$

$$\begin{aligned}Q(\eta)=1&+\frac{[(x+\eta g)^2+\beta^2(y-\eta)^2]^{1/2}}{x+yg}\\&-\frac{c(\eta)}{4}\frac{\beta^2(y-\eta)-\eta g^2-xg}{(x+yg)^2[(x+\eta g)^2+\beta^2(y-\eta)^2]^{1/2}}(y-\eta)\\&-\frac{c'(\eta)}{4}\frac{[(x+\eta g)^2+\beta^2(y-\eta)^2]^{1/2}}{(x+yg)^2}(y-\eta)\end{aligned} \tag{12}$$

For wings with unswept midchord line, $g=0$. In this case, it can be shown[7] that Eq. (10) is consistent with that given in Ref. 6.

For numerical calculation, the η integration in Eq. (10) is first transformed into an angular coordinate through the cosine relation with interval $(0,\pi)$ and the results reduced to finite sums through midpoint trapezoidal rule. Therefore, for

symmetrical loading condition

$$w(x_i,y_i,0) = -\alpha_i(x_i,y_i,0)$$

$$\approx -\frac{1}{8N}\sum_{k=1}^{N}\Gamma'(\eta_k)\left[\frac{P(\eta_k)}{y_i-\eta_k}-\frac{Q(\eta_k)}{y_i+\eta_k}\right]\sin\phi_k \quad (13)$$

where α_i is the induced angle of attack and

$$\eta_k = (1-\cos\phi_k)/2 \quad \phi_k = (2k-1)\pi/2N \quad (k=1,\ldots,N) \quad (14)$$

$$y_i = (1-\cos\phi_i)/2 \quad \phi_i = i\pi/N \quad (i=0,\ldots,N-1) \quad (15)$$

The above integration method has been shown to give quite accurate results for integrals with Cauchy singularity.[8] For wings with partial span flaps, the semispan should be divided into segments along the flap edges with each segment transformed into $(0,\pi)$ interval on the ϕ plane before the midpoint trapezoidal rule is applied.

With the induced angle of attack evaluated at each control station, y_i, Eq. (1) can now be written in a form for successive approximation. First, Eq. (2) is written as

$$\alpha_e(y)^{(n+1)} = \alpha(y) - h\alpha_i^{(n)} - (\alpha_i^{(n+1)} - h\alpha_i^{(n)}) \quad \alpha_i^{(1)} = 0 \quad (16)$$

where $0<h\leq 1$. Using Eq. (16), Eq. (1) can be expanded in a Taylor series. Retaining only up to the linear terms, it is obtained that

$$\beta\Gamma(y)^{(n+1)} \approx c(y)c_l(\alpha - h\alpha_i^{(n)})/2$$
$$-c(y)c_{l_\alpha}(\alpha - h\alpha_i^{(n)})\ (\alpha_i^{(n+1)} - h\alpha_i^{(n)})/2$$

Or, with $\beta\Gamma^{(n)} = cc_l(\alpha - h\alpha_i^{(n)})/2$

$$\beta\Gamma(y)^{(n+1)} + c(y)c_{l_\alpha}(\alpha - h\alpha_i^{(n)})\alpha_i^{(n+1)}$$
$$\approx \beta\Gamma(y)^{(n)} + c(y)c_{l_\alpha}(\alpha - h\alpha_i^{(n)})h\alpha_i^{(n)}/2 \quad (17)$$

Equation (17) can be solved for $\Gamma_{(y)}^{(n+1)}$ with the right-hand side given and $\alpha_i^{(n+1)}$ expressed in terms of $\Gamma'^{(n+1)}$ through Eq. (13). This can be done if a) $\Gamma(y_i)$ at the control stations are expressed in terms of $\Gamma(\eta_k)$ at the integration stations and b) $\Gamma'(\eta_k)$ are also expressed in terms of $\Gamma(\eta_k)$. The first problem can be easily solved using Lagrangian interpolation after the square-root singularity at the tips is properly accounted for. $\Gamma'(\eta_k)$ can be expressed in terms of $\Gamma(\eta_k)$ through the following trigonometric interpolation formula derived in Ref. 7.

$$\Gamma'(\eta_k) = \frac{1}{\sin\bar{\phi}_k}\left[\frac{d\phi_k}{d\eta}\sum_{j=1}^{N}\Gamma(\eta_j)G_{kj}\sin\bar{\phi}_j - \Gamma(\eta_k)\cos\bar{\phi}_k\frac{d\bar{\phi}_k}{d\eta}\right] \quad (18)$$

where ϕ_k has been defined in Eq. (14) and

$$\bar{\phi} = \cos^{-1}\eta \quad (19)$$

The factor, G_{kj}, is defined as

$$G_{kj} = \begin{cases} -(\cot\phi_j)/2 & (k=j) \\ (-1)^{k+j}\sin\phi_j/(\cos\phi_j - \cos\phi_k) & (k\neq j) \end{cases} \quad (20)$$

Equation (18) was derived by developing $\Gamma\sin\bar{\phi}$ in a Fourier cosine series, which is then differentiated. It has been shown to provide very accurate results.[7]

After the sectional circulation is obtained, the total lift coefficient can be obtained by integration with midpoint trapezoidal rule.[8] The induced drag coefficient is computed by the farfield approach used by Multhopp.[9]

Numerical Results and Discussions

In the present computer program, the sectional data are input and interpolated through cubic splines. At low angles of attack, or when the section data show smooth stall characteristics, the convergence factor h in Eq. (17) may be taken as unity. In other cases, it should be taken to be less than unity for convergence. For wings with partial-span flaps, a control point is located at each flap edge. At such a control point, the initial approximation to the right-hand side of Eq. (17) will show a jump across the point. To eliminate the discontinuity in the resulting span loading, any jump in the circulation should be added to the right-hand side of Eq. (17) at such a control point during the iteration. This approach is seen to be different from the conventional method where a loading mode involving logarithmic singularity is usually introduced. In Ref. 2, an empirical method was described to alter the section data in such a way that sectional maximum lift coefficient will be continuous at the end of the flap. In the present method, the section data are not modified in any way. When the leading edge is swept and the airfoil section is defined in the streamwise direction, the effective thickness ratio is to be increased in accordance with Weber's theory.[10] Therefore, both the section lift coefficient and the lift curve slope are to be increased according to the following formula for c_l.

$$(c_l)_{\Lambda l.e.\neq 0} = (c_l)_{\Lambda l.e.=0}\frac{[1+(0.8t/c)/\cos\Lambda_{l.e.}]}{(1+0.8t/c)} \quad (21)$$

The aforedescribed method is first applied to a rectangular wing of $AR=10$ with sectional lift curve slope of 2π. The present program can solve Prandtl's equation by setting $P(\eta)=1$ and $Q(\eta)=1$ in Eq. (13). The lift curve slope $C_{L\alpha}$ as calculated by the present Prandtl's method is 5.049 per rad with $N=30$, as compared with 5.047 per rad given by Multhopp's lifting line method. On the other hand, the present improved method gives $C_{L\alpha}=4.803$ per rad with $N=40$, which compares quite favorably with 4.836 per rad by the lifting surface method of Ref. 8.

With the validity of the program verified, it is then applied to a clean swept wing of $AR=6$ and with the quarter-chord sweep of 30 deg. The results are shown in Fig. 1. The experimental results were reported in Ref. 11 and the experimental section data used in the program are taken from Ref. 12. It is seen that significant improvement by the present improved method has been achieved. Figure 2 shows further

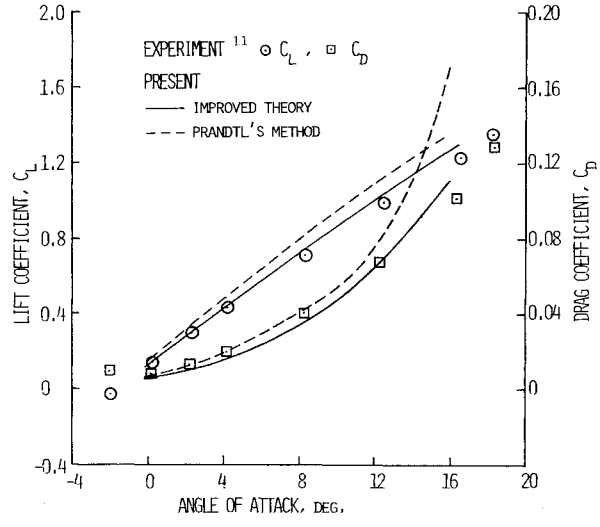

Fig. 1 Comparison of theories with experiment: $\Lambda_{c/4}=30$ deg, $AR=6$, $\lambda=0.5$, $M_\infty=0$, and $N=40$.

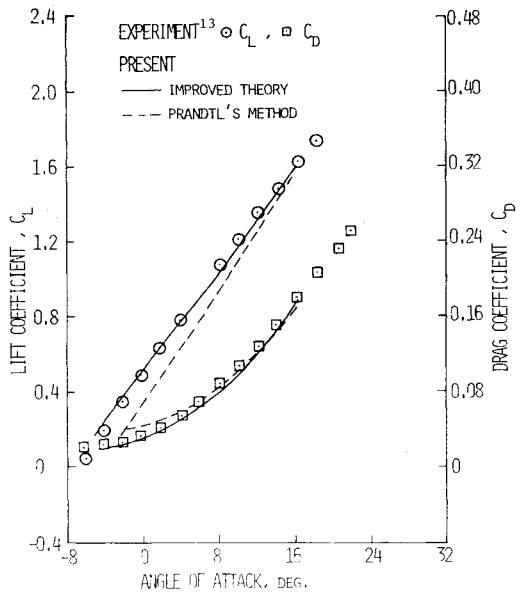

Fig. 2 Comparison of theories with experiment for a wing with partial-span flap: 50% inboard flap span, $AR = 6$, $\lambda = 0.5$, $\Lambda_{c/4} = 9.67$ deg, $M_\infty = 0$, and $N = 40$.

comparison of the theories for a wing of $AR = 6$ with 50% inboard flap span. The flapped section data are given in Ref. 13 and the clean section data are taken from Ref. 12. Again, the present improved method predicts results in good agreement with experiment. Prandtl's method is seen to produce lower lift in this case. Examination of the numerical results indicates that while Prandtl's theory produces slightly lower downwash over the flapped span, it gives much lower upwash over the outboard clean span which is due to the strong trailing vortices from the inboard flapped section. This is probably the aspect-ratio effect, because as the aspect ratio is increased to 10, Prandtl's theory predicted higher lift.

Concluding Remarks

An improved nonlinear lifting-line theory has been presented with applications. The new theory, which allows the use of nonlinear section data, predicts aerodynamic characteristics of wings of moderate to high aspect ratios with or without sweep in better agreement with experiment than Prandtl's theory. The theory can be used to convert the airfoil characteristics to wing characteristics.

Acknowledgment

This investigation was supported by University of Kansas General Research allocation No. 3839-5038.

References

[1] Sivells, J. C. and Neely, R. H., "Method for Calculating Wing Characteristics by Lifting-Line Theory Using Nonlinear Section Lift Data," NACA Rept. 865, 1947.

[2] Sivells, J. C. and Westrick, G. C., "Method for Calculating Lift Distributions for Unswept Wings with Flaps or Ailerons by Use of Nonlinear Section Lift Data," NACA Rept. 1090, 1952.

[3] McVeigh, M. A. and Kisielowski, E., "A Design Summary of Stall Characteristics of Straight Wing Aircraft," NASA CR-1646, 1971.

[4] Smetana, F.O., Summey, D.C., Smith, N.S., and Carden, R. K., "Light Aircraft Lift, Drag and Moment Prediction – A Review and Analysis," NASA CR-2523, 1975.

[5] Weissinger, J., "The Lift Distribution of Swept-Back Wings," NACA TM 1120, 1947.

[6] Lan, C., "An Improved Nonlinear Lifting-Line Theory," *AIAA Journal*, Vol. 11, May 1973, pp. 739-742.

[7] Fasce, M. H., "Applications of an Improved Nonlinear Lifting-Line Theory," M. S. Thesis, Department of Aerospace Engineering, University of Kansas, March 1975.

[8] Lan, C. E., "A Quasi-Vortex-Lattice Method in Thin Wing Therory," *Journal of Aircraft*, Vol. 11, Sept. 1974, pp. 518-527.

[9] Multhopp, H., "Methods for Calculating the Lift Distribution of Wings (Subsonic Lifting-Surface Theory)," British ARC R&M 2884, 1950.

[10] Weber, J., "The Calculation of the Pressure Distribution over the Surface of Two-Dimensional and Swept Wings with Symmetrical Aerofoil Sections," British ARC, R&M 2918, 1953.

[11] Anderson, R. F., "Determination of the Characteristics of Tapered Wings," NACA Rept. 572, 1936.

[12] Abbot, I. H. and Von Doenhoff, A. E., *Theory of Wing Sections*, Dover, New York, 1959.

[13] Pearson, H. A. and Anderson, R. F., "Calculation of the Aerodynamic Characteristics of Tapered Wings with Partial-Span Flaps," NACA Rept. 665, 1939.

Prediction of Tethered-Aerostat Response to Atmospheric Turbulence

James DeLaurier*
Institute for Aerospace Studies, University of Toronto, Toronto, Canada

Introduction

WITHIN recent years, aerodynamically shaped tethered balloons (aerostats) have been used as "skyhooks" and instrument-carrying elevated platforms. For example, the skyhook applications have included balloon logging[1] and experiments in ship-cargo unloading[2]; platform applications include telecommunications relay,[3] optical surveillance,[4] and atmospheric measurements.[5]

For all of these examples, the operational advantages of utilizing an aerostat are compromised by its inherent unsteadiness in atmospheric turbulence. A tethered-aerostat system is useful only if this unsteadiness is small enough to allow it to perform its tasks.

In 1970, DeLaurier[6] developed an analysis by which the first-order station-keeping stability of a tethered aerostat could be predicted. This was applied to the configuration design of the Family-II aerostat (Fig. 1), and experiments confirmed the theoretical predictions of first-order stability throughout its flight envelope.[7] However, first-order stability only guarantees steadiness in steady winds. Although it is a necessary condition for minimal response to turbulence, it is not sufficient.

In order to address this problem, DeLaurier[8] developed an analysis by which the rms lateral response of a tethered aerostat may be predicted. This Note describes the development of a corresponding longitudinal analysis, and the application of both analyses to an example Family-II aerostat.

Method of Analysis

The spectral approach was used for this work, where the cable-aerostat system's transfer functions to a spectral component of turbulence were combined with an atmospheric-turbulence power-spectrum function to obtain power functions of the system's responses. Then, by integration, mean square values for the responses were obtained. This is analogous to the aircraft turbulence-response analysis described by Etkin,[9] where turbulence was considered to be "frozen" with respect to the atmosphere, and the vehicle was excited by flying through it.

Received Oct. 26, 1976.

Index categories: Aircraft Gust Loading and Wind Shear; Aircraft Handling, Stability, and Control; Aircraft Performance.

*Associate Professor.